

# An Investigation of Dynamic Dark Energy Models via an Analysis of Type 1a Supernovae

Bradley Makinson  
L3 Computing Project, Tutorial Group C1  
Submitted: October 2, 2024

We determine cosmological constraints for a variety of dark energy models by fitting the distance modulus-redshift relation to the SCP Union2.1 dataset via Markov-Chain Monte-Carlo techniques, with the aim of determining any statistically significant deviation from the cosmological constant model. We first determine constraints on the cosmological density parameters for the  $\Lambda$ CDM model, with no restriction on Universe geometry, of  $\Omega_{\Lambda,0} = 0.72 \pm 0.08$  and  $\Omega_{M,0} = 0.28 \pm 0.06$ , providing evidence for a geometrically flat Universe. We then carry forward this flat Universe result as an additional restriction when determining constraints for a range of alternative, dynamical dark energy models, for which we find no deviation from the  $\Lambda$ CDM model within one standard deviation when only supernova data is included in the analysis. We then include CMB and BAO measurements as priors to provide tighter constraints, after which it was found that the  $w$ CDM and Efstathiou models showed deviations from the  $\Lambda$ CDM model at the  $1\sigma$  significance level, indicating a preference for dynamical dark energy densities. We conclude that a larger dataset containing supernovae at higher redshifts is required to constrain the cosmological parameters sufficiently such that these results could be investigated more conclusively at the  $> 2\sigma$  significance level.

## I. Introduction and Theory

The analysis of type 1a supernovae has become one of the most powerful and widely used methods of studying cosmology, providing constraints on the density and nature of dark energy, and the abundances of different matter species in the Universe. From early studies of type 1a supernovae [1][2], it was discovered that the expansion rate of the Universe is accelerating, requiring a form of energy with negative pressure to account for this accelerating expansion, namely dark energy, which contributes to  $\sim 70\%$  [1] of the present day contents of the Universe. The density of dark energy was initially introduced as a cosmological constant from Einstein's Theory of General Relativity. However, the cosmological coincidence problem [3] has prompted an investigation of dynamical dark energy models, where the dark energy density is not a constant in time, but is instead a function of redshift. More recent type 1a supernova samples containing data at sufficiently large redshifts, such as the Supernova Cosmology Project (SCP) [4], Joint Light Curve Analysis (JLA) [5], and the Pantheon+ sample [6], have allowed for an investigation of dynamical dark energy models which deviate from a cosmological constant [7]. In this work, we use the SCP Union2.1 dataset [4] containing 580 type 1a supernovae, spanning a range of redshifts  $0.01 < z < 1.41$ , alongside Cosmic Microwave Background (CMB) [8] and Baryonic Acoustic Oscillation (BAO) [9] measurements to perform an analysis of various dark energy models with the aim of determining any significant deviation from the cosmological constant.

Type 1a supernovae often occur in a binary system, where a white dwarf accretes mass from its companion until its mass exceeds the Chandrasekhar limit, at which point the outward pressure provided by electron degeneracy becomes insufficient and the white dwarf collapses under its own gravity. Type 1a supernovae have a characteristic peak magnitude as the collapse always takes place when the white dwarf reaches a fixed mass, making them standardisable candles [10]. It is the knowledge of this peak magnitude which makes type 1a supernovae incredibly useful in cosmological studies.

One key class of cosmological parameters we use type 1a supernovae to determine are the cosmological density parameters, which represent the relative abundances of different matter species within the Universe, and are defined as a ratio of the density of a given matter species to some

critical density:

$$\Omega_i = \frac{\rho_i(a)}{\rho_{\text{crit}}(a)}, \quad (1)$$

$$\rho_{\text{crit}}(a) = \frac{3H^2(a)}{8\pi G}, \quad (2)$$

where  $i$  denotes the matter species ( $i = M, R, DE$  for matter, radiation, and dark energy, respectively),  $H(a)$  is the Hubble parameter,  $a$  is the scale factor, defined by  $a = 1/(1+z)$  where  $z$  is the cosmological redshift, and  $G$  is Newton's Gravitational Constant ( $G = 6.674 \times 10^{11} \text{Nm}^2\text{kg}^{-2}$  [11]). An accurate determination of these density parameters is central to the study of cosmology, allowing the expansion history and future evolution of the Universe to be extrapolated from the Friedmann equation, one form of which is given below:

$$H^2(a) = \frac{H_0^2 \Omega_{R,0}}{a^4} + \frac{H_0^2 \Omega_{M,0}}{a^3} + H_0^2 \Omega_{DE,0} f_{DE}(a) - \frac{kc^2}{R_0^2 a^2}, \quad (3)$$

where  $c$  is the speed of light in vacuum ( $c = 2.998 \times 10^8 \text{m s}^{-1}$  [12]),  $H_0$  is the Hubble constant,  $k$  is a dimensionless constant which depends on the geometry of the Universe,  $R_0$  is the curvature scale factor, and  $f_{DE}(a)$  represents the functional form of the dark energy density, such that  $f_{DE}(a) = \rho_{DE}(a)/\rho_{DE,0}$ . The curvature constant  $k$  can take one of three values:  $k = -1$  for an open universe, where  $\Omega_0 = \Omega_{R,0} + \Omega_{M,0} + \Omega_{DE,0} < 1$ ,  $k = 0$  for a flat universe, where  $\Omega_0 = 1$ , and  $k = 1$  for a closed universe, where  $\Omega_0 > 1$ . The subscript '0' denotes the present-day value. By evaluating Eq. (3) at the present day, where  $a = 1$ , and rearranging, it can be found that the curvature scale factor is given by

$$R_0 = \frac{c}{H_0} (|\Omega_{R,0} + \Omega_{M,0} + \Omega_{DE,0} - 1|)^{-1/2}. \quad (4)$$

Recent studies have determined that the present day radiation density parameter,  $\Omega_{R,0}$ , is of order  $10^{-5}$  [13], so for the purposes of this study it can be considered negligible and hence can be excluded from the above equations.

There are several different forms that  $f_{DE}(a)$  can take depending on the model of dark energy being investigated. Each dark energy model can be parameterized by its dimensionless equation of state parameter,  $w$ , defined as:

$$w = P_{DE}/\rho_{DEC}^2, \quad (5)$$

**TABLE I.** The five dark energy models we investigate, along with their corresponding equations of state and functional forms.

Model	$w(z)$ [14]	$f_{DE}(z)$ [14]
$\Lambda$ CDM	-1	1
$w$ CDM	$w_0$	$(1+z)^{3(1+w_0)}$
CPL	$w_0 + w'(z=0) \frac{z}{(1+z)}$	$(1+z)^{3(1+w_0+w'(z=0))} \exp\left(-\frac{3w'(z=0)z}{1+z}\right)$
JBP	$w_0 + w'(z=0) \frac{z}{(1+z)^2}$	$(1+z)^{3(1+w_0)} \exp\left(-\frac{3w'(z=0)}{2} \left(\frac{z}{1+z}\right)^2\right)$
Efstathiou	$w_0 + w'(z=0) \ln(1+z)$	$(1+z)^{3(1+w_0)} \exp\left(-\frac{3w'(z=0)}{2} (\ln(1+z))^2\right)$

where  $P_{DE}$  is the dark energy pressure, and  $\rho_{DE}$  is the dark energy density. A wide variety of dark energy models have been theorised, but in this work we will focus on five of the most well-known: the  $\Lambda$ CDM,  $w$ CDM, Chevallier-Polarski-Linder (CPL), Jassal-Bagla-Padmanabhan (JBP), and Efstathiou models [14]. The equation of state for each of these models is given in Table I, where  $w_0$  is the present day value of the equation of state parameter, and  $w'(z=0)$  is its first order derivative at  $z=0$ . Through the cosmic energy equation [15], the functional form of the dark energy densities for each model can be derived [14], as given in the final column of Table I. For the  $\Lambda$ CDM model, we denote the present-day dark energy density as  $\Omega_{\Lambda,0}$  to be consistent with literature.

## II. Methods

In this work, we use a Markov-Chain Monte-Carlo (MCMC) algorithm to determine constraints on the cosmological parameters for each of the dark energy models given in Table I.

### A. Model Function

To determine cosmological parameters via MCMC, we first need to define a model function that we can use to constrain the parameters of interest. The model function we use in this work relates distance modulus and redshift in accordance with the Union2.1 dataset. The distance modulus-redshift relation is given by:

$$\mu = m - M = 5 \log_{10}(d_L) - 5, \quad (6)$$

where  $d_L$  is the luminosity distance in units of parsecs,  $m$  is the object's apparent magnitude, and  $M$  is the it's absolute magnitude. The luminosity distance can be expressed in terms of the Friedmann-Walker-Robertson (FRW) metric,  $S_k(r_c)$ :

$$d_L = (1+z)S_k(r_c), \quad (7)$$

where  $S_k(r_c)$  is defined by:

$$S_k(r_c) = \begin{cases} R_0 \sin(r_c/R_0) & \text{if } k = 1 \\ r_c & \text{if } k = 0 \\ R_0 \sinh(r_c/R_0) & \text{if } k = -1 \end{cases} \quad (8)$$

and the comoving distance,  $r_c$ , is given by:

$$r_c = c \int_0^z \frac{dz'}{H(z')}. \quad (9)$$

Since this integral does not have a general analytic solution, we calculate it numerically using the 'scipy.integrate.quad' function within the 'scipy.integrate' package in Python, with an absolute error tolerance of  $\sim 10^{-8}$ . The precision of this function is discussed in section III.

By combining equations (3), 4, (6), (7), (8), and (9), we obtain a distance modulus-redshift relation containing the cosmological parameters of interest for the various dark energy models. It should be noted that the Union2.1 dataset has assumed a value of  $H_0 = 70 \text{ km s}^{-1} \text{ Mpc}^{-1}$  for the Hubble constant, so we will assume the same value throughout this work.

### B. Markov-Chain Monte-Carlo (MCMC)

Markov-Chain Monte-Carlo (MCMC) is a random sampling method which is used widely for the purpose of determining unknown parameters in a model and their uncertainty. It is comprised of two key concepts; Markov-Chain and Monte-Carlo. We follow the work of Ottoson [16] by first introducing these concepts separately and then combining them in the relevant context.

A Markov-Chain is a stochastic process that describes a sequence of discrete random steps in which each step is dependent only on the previous step. More mathematically, the conditional probability of each step is dependent on the previous step only.

The Monte-Carlo method is a repeated, random sampling process that can be used to solve deterministic problems where an analytic solution is not feasible. There are a wide range of Monte-Carlo approaches, all of which follow a general process similar to that outlined in Fig. 1.

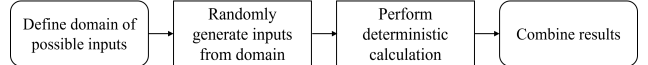


**FIG. 1.** Flowchart illustrating the steps generally involved in a Monte-Carlo algorithm [16].

These two techniques can be combined to create the MCMC algorithm, where a posterior distribution is repeatedly and randomly sampled under constraints from a likelihood function and prior distribution. The random nature of the sampling shows the 'Monte-Carlo' part of the algorithm, and the fact that this sampling is constrained encodes the 'Markov-Chain' aspect. With a dataset  $y$  and model parameters  $\theta$ , Bayes' rule [16] can be written as:

$$p(\theta|y) = \frac{p(y|\theta)p(\theta)}{p(y)} \quad (10)$$

where the posterior distribution,  $p(\theta|y)$ , represents the conditional probability of a set of model parameters being correct given the dataset. The marginal probability,  $p(y)$ , is not dependent on the model parameters, and so can simply be considered as a normalization factor, meaning the posterior distribution is proportional to the product of the likelihood function,  $p(y|\theta)$ , and the prior distribution,  $p(\theta)$ . The likelihood function can be taken as a Gaussian distribution that is dependent on the  $\chi^2$  statistic:

$$p(y|\theta) \propto \exp\left(-\frac{1}{2}\chi^2\right). \quad (11)$$

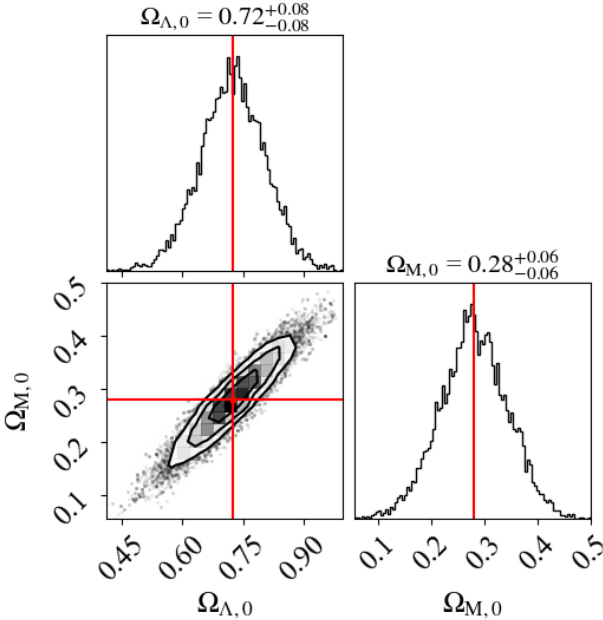


**FIG. 2.** Constraints on the cosmological density parameters with uniform priors for the  $\Lambda$ CDM model (non-zero curvature allowed). This figure shows both contour plots to illustrate the correlation between the parameters, with contours at 0.5, 1, 1.5, and 2 standard deviations, and marginalised probability distributions for each parameter. The red lines indicate the 50th percentile.

Initially, we use uniform priors in the range [0, 1] for the density parameters, [-5, 1] for  $w_0$ , and [-5, 5] for  $w'(z = 0)$  where applicable, which encapsulate a large percentage of the confidence region. Gaussian prior distributions constructed from CMB [8] and BAO [9] measurements can also be used to provide additional constraints on the posterior distribution [17].

We use the Python library 'emcee' in this work to carry out the MCMC process, with 32 random walkers each traversing parameter space for 1000 steps. Each of these walkers is assigned an initial position given by randomly sampling the uniform priors given above, and traverses parameter space until it converges to the region of highest probability (the region in parameter space where  $|\chi^2 - \chi^2_{\min}| \lesssim 1$ ). We choose the first 400 steps as 'burn-in' time, during which we assume the algorithm is converging to the region of highest probability. These steps are therefore discarded. We use the above number of walkers and steps to provide a good balance between convergence and computational time - the convergence of this process will be discussed in section III. We then use the 'corner' library to produce corner plots that show both the correlation between parameters and the marginalised probability distributions for each parameter. The best fit value and uncertainties can then be calculated from the 16th, 50th, and 84th percentiles. These percentiles were chosen such that the reported uncertainties represent one standard deviation ( $\sigma$ ) from the 50th percentile.

It should be noted that MCMC is a random sampling algorithm, not a deterministic optimisation algorithm - it will produce slightly different results each time it is ran. Hence, the results quoted in this paper should not be taken as the absolute best-fit values - they are the 50th percentile of a number of random samples from a posterior distribution, constructed by maximising the likelihood function subject to constraints from a prior distribution.

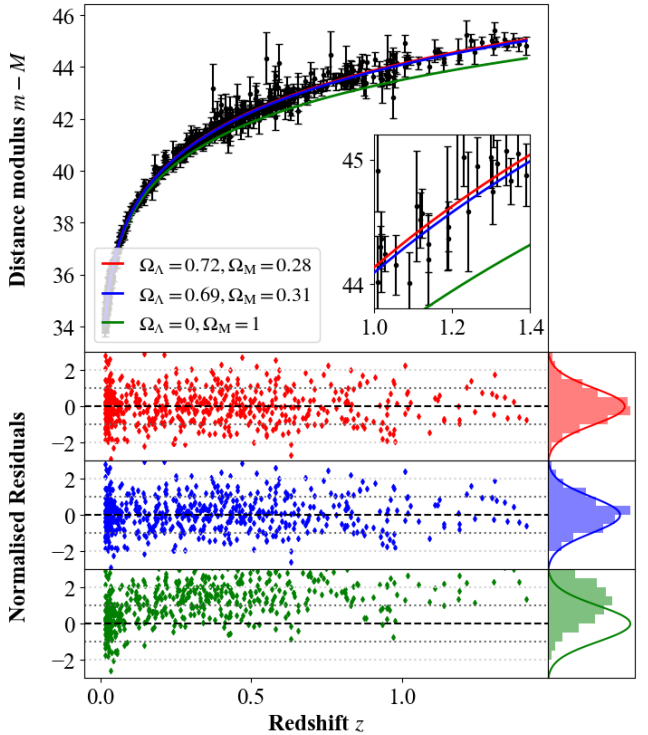


**FIG. 3.** The distance modulus-redshift relations for  $\Lambda$ CDM models containing values for the cosmological density parameters determined in this work from supernova data only (red), and supernova+CMB+BAO data (blue). There is also a model shown in green for a Universe in which there is no dark energy to illustrate both the existence of dark energy, and how the sensitivity of the model function to changes in the density parameters increases with redshift. The Union 2.1 data is represented by the black data points, with their corresponding error bars. The subplot is a zoomed in region of the above for the range of redshifts  $1.0 < z < 1.4$  to help the reader resolve the differences between the models. Below are three normalised residual plots with their corresponding normalised residual histogram, each of which are colour coded accordingly.

Finally, we compare the results given by MCMC to those from an optimisation algorithm, namely 'scipy.optimize.curve\_fit', to confirm their validity. This optimisation algorithm utilises the method of non-linear least squares to determine the best-fit values of unknown parameters in a model, and can provide estimates for their uncertainties via the diagonalisation of the resulting covariance matrix. We choose the initial parameter values for the optimisation algorithm to be those determined by MCMC to prevent it from getting stuck in local minima.

### III. Results and Discussion

#### A. Dark Energy Models

Fitting the Union2.1 dataset to the  $\Lambda$ CDM model with the uniform priors outlined in section II, we determine values of  $\Omega_{\Lambda,0} = 0.72 \pm 0.08$  and  $\Omega_{M,0} = 0.28 \pm 0.06$ , which are in agreement within one standard deviation with the combined CMB and BAO values for the base- $\Lambda$ CDM model given by the Planck Collaboration of  $\Omega_{\Lambda,0}^{\text{Planck}} = 0.689 \pm 0.006$  and  $\Omega_{M,0}^{\text{Planck}} = 0.311 \pm 0.006$  [8]. The marginalised probability distributions for each of the parameters are shown in Fig. 2, and it can be seen that they closely represent a Gaussian, implying that both parameters are constrained within the prior ranges. This model gives a reduced  $\chi^2$  of 0.97, and a p-value of 0.67. Since  $p > 0.05$  and  $\chi^2_{\text{red}} \approx 1$ , we

**TABLE II.** Constraints for each of the dark energy models outlined in Table I, obtained by applying an MCMC fitting algorithm to the Union 2.1 dataset, where the reported uncertainties represent one standard deviation. Results are given for both uniform and CMB+BAO priors. The last two columns quantify the validity of the fit by reporting both the reduced  $\chi^2$  and p-values for each model. 'N/A' indicates that the parameter was not fitted in that model.

Model	Priors	$\Omega_{\text{DE},0}$	$\Omega_{\text{M},0}$	$w_0$	$w'(z = 0)$	$\chi^2_{\text{red}}$	p value
$\Lambda\text{CDM}$	Uniform	$0.72 \pm 0.08$	$0.28 \pm 0.06$	N/A	N/A	0.97	0.67
$\Lambda\text{CDM}$	CMB+BAO	$0.691^{+0.006}_{-0.005}$	$0.308 \pm 0.005$	N/A	N/A	0.98	0.61
Flat $w\text{CDM}$	Uniform	$0.72^{+0.07}_{-0.06}$	N/A	$-1.01^{+0.14}_{-0.16}$	N/A	0.97	0.67
Flat $w\text{CDM}$	CMB+BAO	$0.70 \pm 0.01$	N/A	$-1.06 \pm 0.04$	N/A	0.97	0.67
Flat CPL	Uniform	$0.65^{+0.10}_{-0.06}$	N/A	$-1.05^{+0.13}_{-0.15}$	$-1.05^{+1.47}_{-2.15}$	0.98	0.65
Flat CPL	CMB+BAO	$0.66 \pm 0.03$	N/A	$-1.07 \pm 0.11$	$-0.88^{+1.02}_{-1.23}$	0.97	0.66
Flat JBP	Uniform	$0.68^{+0.13}_{-0.07}$	N/A	$-1.00^{+0.12}_{-0.17}$	$-0.69^{+1.84}_{-2.43}$	0.98	0.65
Flat JBP	CMB+BAO	$0.68 \pm 0.03$	N/A	$-1.02^{+0.11}_{-0.13}$	$-1.03^{+1.44}_{-1.53}$	0.98	0.65
Flat Efstathiou	Uniform	$0.63^{+0.09}_{-0.05}$	N/A	$-1.07^{+0.13}_{-0.14}$	$-1.56^{+1.65}_{-2.08}$	0.98	0.66
Flat Efstathiou	CMB+BAO	$0.65 \pm 0.03$	N/A	$-1.06 \pm 0.11$	$-0.97^{+0.87}_{-1.14}$	0.97	0.66

conclude that this model is a good fit to the data and hence the determined parameters are valid. Additionally, as seen in Fig. 3, the normalised residuals for this model show no noticeable pattern and their histogram closely represents a Gaussian distribution, providing further evidence that this model produces a good fit to the data.

However, our derived parameters are not as tightly constrained as those from CMB and BAO studies. This is most likely due to the significant correlation between the two density parameters seen in Fig 2. This prompts us to use CMB and BAO measurements as priors to provide tighter constraints and remove the degeneracy between parameters, achieving results of  $\Omega_{\Lambda,0} = 0.691 \pm 0.006$  and  $\Omega_{\text{M},0} = 0.308^{+0.005}_{-0.006}$ . These results give  $\chi^2_{\text{red}} = 0.98$ ,  $p = 0.61$ , and a Gaussian distribution of normalised residuals, implying that the new parameter values also provide a good fit to the data. Additionally, these results give a total density parameter of  $\Omega_0 = 0.999 \pm 0.008$ , which is consistent with a geometrically flat Universe. As can be seen in Fig. 3, the model function becomes increasingly sensitive to changes in the density parameters at higher redshifts, leading us to conclude that our derived density parameters would be further constrained if additional supernova data at higher redshifts was included in the analysis.

We then fit the Union2.1 dataset to the  $w\text{CDM}$  model with uniform priors, and an additional condition that the Universe must have zero curvature (i.e.  $\Omega_{\text{M},0} + \Omega_{\text{DE},0} = 1$ ). This condition was added to help the algorithm sufficiently constrain the model parameters and hence provide meaningful results. We obtain values of  $\Omega_{\text{DE},0} = 0.72^{+0.07}_{-0.06}$  and  $w_0 = -1.01^{+0.14}_{-0.16}$ , which are consistent to well within one standard deviation with those given in the Union2.1 release paper [4] for supernova data only, providing evidence that our MCMC algorithm is functioning correctly. Adding CMB+BAO priors, we determine values of  $\Omega_{\text{DE},0} = 0.70 \pm 0.01$  and  $w_0 = -1.06 \pm 0.04$ . With uniform priors, we obtain results which are consistent with the  $\Lambda\text{CDM}$  model within one standard deviation, but when CMB+BAO priors are added, the parameter uncertainties are reduced sufficiently such that a  $> 1\sigma$  deviation from the  $\Lambda\text{CDM}$  model can be resolved for the  $w_0$  parameter, indicating that the  $w\text{CDM}$  model has a preference for a dynamical dark energy density at the  $1\sigma$  significance level. Since  $w_0 < -1$ , the algorithm has converged to a region in the phantom regime [17] for which the dark energy density decreases with redshift, as can be deduced from the functional form given in Table I. This is a physically reasonable result as it is compatible with

the radiation- and matter-dominated eras theorised at larger redshifts.

The Union 2.1 dataset will become increasingly unsuitable at providing tight constraints as the dimensionality of parameter space is increased due to the inherent degeneracy between the cosmological parameters. Hence, we carry forward the zero curvature condition for the remaining dynamical dark energy models to reduce the number of fit parameters from four to three, as a flat Universe only necessitates a determination of one density parameter rather than both. The results for each of the dynamical dark energy models outlined in Table I is shown in Table II, along with their reduced  $\chi^2$  and p-value statistics. One can see that all derived models provide a good fit to the data for the same reasons as previously. Additionally, the CPL and JBP models agree within one standard deviation with the  $\Lambda\text{CDM}$  model, in which  $w_0 = -1$  and  $w'(z = 0) = 0$ , both with and without CMB+BAO priors. This is important as it shows that even when we allow these models the freedom to deviate from the  $\Lambda\text{CDM}$  model, the determined parameters still reduce them to the  $\Lambda\text{CDM}$  model. The most interesting result can be seen with the Efstathiou model when we include CMB+BAO priors, in which we determine  $w'(z = 0) = -0.97^{+0.87}_{-1.14}$ , which does not agree with the fixed  $\Lambda\text{CDM}$  value of 0 within one standard deviation. Since this value is negative, we conclude that the Efstathiou model has a preference for a dark energy density which increases with redshift. We come to this conclusion because, from the functional form of the dark energy density for the Efstathiou model in Table I, it can be deduced that negative  $w'(z = 0)$  values result in exponential-like growth of the dark energy density with redshift. Whilst this result seems physically unreasonable, as it is in direct contradiction with the widely accepted idea that the Universe was radiation-dominated in its infancy, it should be noted that we are only fitting to supernova data up to redshifts of  $\sim 1.4$ , and hence this exponential-like growth should only be taken as valid up to that redshift. Furthermore, as can be seen in Fig. 4, there is a significant curved degeneracy in the  $\Omega_{\text{DE},0} - w'(z = 0)$  contours, producing large uncertainties in the  $w'(z = 0)$  parameter, and thus highlighting the need for additional supernova data at higher redshifts to provide tighter constraints on the parameters, allowing us to confirm more conclusively (at the  $> 2\sigma$  significance level) the possibility of an increasing dark energy density for the Efstathiou model.

Additionally, upon closer inspection, whilst all other models agree within one standard deviation with the  $\Lambda\text{CDM}$

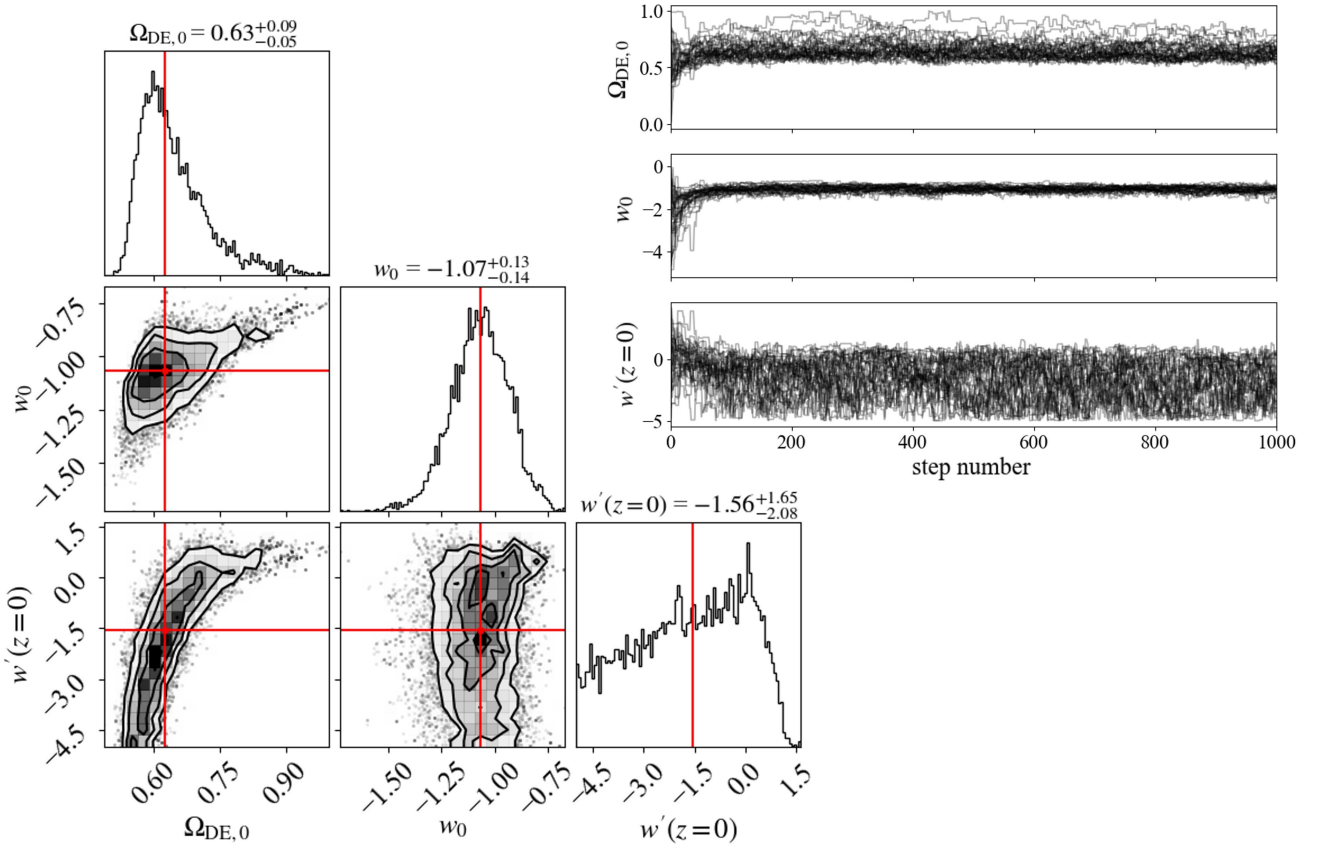


**FIG. 4.** Constraints on the Efstathiou dark energy model with uniform priors under the assumption of a flat Universe. Left: Contour plots to illustrate the correlation between parameters, with contours at 0.5, 1, 1.5, and 2 standard deviations, as well as marginalised posterior probability distributions for each parameter. The red lines indicate the 50th percentile. Right: The position of each random walker as a function of the number of steps, illustrating the convergence of the MCMC algorithm after around 100 steps.

**TABLE III.** A comparison of the results from MCMC and the optimum value returned by ‘scipy.optimize.curve\_fit’ for the  $\Lambda$ CDM model using supernova data only.

Parameter	MCMC result	Optimum value
$\Omega_{\Lambda,0}$	$0.72 \pm 0.08$	$0.72 \pm 0.08$
$\Omega_{M,0}$	$0.28 \pm 0.06$	$0.28 \pm 0.06$
$\chi^2_{red}$	0.973	0.973

model, there is a clear preference for negative  $w'(z = 0)$  values across all models, which is also seen in other recent cosmological studies [7][8]. Once again, additional data at higher redshifts would provide the tighter constraints necessary to resolve any deviations from the  $\Lambda$ CDM model at the  $1\sigma$  significance level for these models.

This additional data would also allow for a sufficiently constrained analysis of the various dynamical models without the assumption of a flat Universe. Whilst each of the results in Table II provide a statistically good fit to the data, and there is convincing evidence in the literature for a geometrically flat Universe, it remains a possibility that a better fit exists for which the density parameters do not sum to one, and hence the Universe is not flat. This assumption could therefore be a reason behind the deviation from the  $\Lambda$ CDM model seen for some of the dynamical models in this report, as there may be better fits that exist which do reduce to the  $\Lambda$ CDM model within one standard deviation, but instead indicate a preference for a non-flat Universe.

### B. Numerical Convergences

As outlined in section II, the ‘scipy.integrate.quad’ function was used to numerically perform the integration in Eq.

**TABLE IV.** A comparison of the results from MCMC and the optimum value returned by ‘scipy.optimize.curve\_fit’ for the flat Efstathiou model using supernova data only.

Parameter	MCMC result	Optimum value
$\Omega_{DE,0}$	$0.63^{+0.09}_{-0.05}$	$0.73 \pm 0.44$
$w_0$	$-1.07^{+0.13}_{-0.14}$	$-0.99 \pm 0.50$
$w'(z = 0)$	$-1.56^{+1.65}_{-2.08}$	$0.09 \pm 3.38$
$\chi^2_{red}$	0.975	0.974

(9), as this integral could not be solved analytically. The absolute fractional error returned by ‘scipy.integrate.quad’ for this integral was averaged over all redshifts in the dataset, giving a fractional error of  $\sim 10^{-14}$  for all models. This is most likely due to numerical round-off, and is so small that it can be considered negligible as a source of systematic error.

The convergence of the MCMC algorithm can be investigated by plotting the positions of each random walker in parameter space as a function of the number of steps. As mentioned previously, each of the walkers starts at a position in parameter space given by randomly sampling the uniform priors outlined in section II. It can be seen from Fig. 4 that after less than 100 steps, each of these walkers has converged to the region of highest probability. Similar convergences can be seen for all other dark energy models in appendix A. This validates our choice of 1000 steps, and confirms 400 discarded ‘burn-in’ steps is more than enough to cover the convergence region.

When comparing the MCMC results to those returned by ‘scipy.optimize.curve\_fit’, we see that for the  $\Lambda$ CDM model in Table III, the MCMC results agree with those returned by the optimisation algorithm, indicating that

our MCMC algorithm is indeed converging to the correct region in parameter space. However, when inspecting the comparison for the Efstathiou model in Table IV, we see that there is a discrepancy of around one standard deviation for all parameters. This indicates that when the parameters are poorly constrained and there is significant degeneracy between parameters, as can be seen for the Efstathiou model in Fig. 4, the MCMC algorithm has a higher probability of deviating further from the absolute best-fit values given by optimisation algorithms. The fact that the MCMC algorithm has still produced results which give a reduced  $\chi^2$  value of 0.975 despite this discrepancy further illustrates the degeneracy between the model parameters. It can also be seen from Table IV that MCMC provides tighter constraints, perhaps due to the covariance matrix overestimating the uncertainties as a result of the significant correlation between parameters. This validates the choice of MCMC as our primary method.

#### IV. Conclusions and Further Work

In this work, we used MCMC techniques to fit the distance modulus-redshift relation to the Union2.1 dataset in order to obtain constraints on various cosmological parameters. We first determined constraints on the cosmological density parameters for the  $\Lambda$ CDM model, obtaining results of  $\Omega_{\Lambda,0} = 0.691 \pm 0.006$  and  $\Omega_{M,0} = 0.308^{+0.005}_{-0.006}$  when CMB+BAO priors are included, which are consistent with a geometrically flat Universe within one standard deviation. We then carried this flat Universe result forward when investigating several alternative, dynamical dark energy models to reduce the number of fit parameters and thus obtain better constraints. We find that all dynamical dark energy models show no deviation from the  $\Lambda$ CDM model within one standard deviation when only Union2.1 supernova data is used. When we include CMB and BAO priors to provide additional constraints, we find  $w_0 = -1.06 \pm 0.04$  for the  $w$ CDM model, and  $w'(z = 0) = -0.97^{+0.87}_{-1.14}$  for the Efstathiou model, neither of which agree with the  $\Lambda$ CDM values of  $w_0 = -1$  and  $w'(z = 0) = 0$  within one standard deviation. From inspecting the functional forms of the dark energy density in each case, we concluded that the  $w$ CDM/Efstathiou models indicated a preference for a dark energy density which decreases/increases with redshift. We then confirmed the validity of our MCMC algorithm by illustrating its convergence and comparing the results it gives to those from an optimisation algorithm, finding that the discrepancy between the two becomes larger in parameter spaces with higher dimensionality and greater parameter degeneracy.

Larger type 1a supernova datasets have been released in recent years, such as the Pantheon+ sample [6] which contains 1550 type 1a supernovae up to redshifts of 2.26. By utilising larger datasets such as this, tighter constraints on the cosmological parameters can be achieved, thus reducing the derived uncertainties and making it easier to resolve potential deviations from the  $\Lambda$ CDM model at the  $> 1\sigma$  significance level. It was noted that tighter constraints would also allow for an investigation of dynamical dark energy models with no restriction on Universe geometry, where the density parameters can vary independently. Removing this restriction could allow the MCMC algorithm to find a better fit to the data in which the Universe geometry is not flat.

#### Acknowledgments

The author would like to thank Prof. Cedric Lacey for supervising this project and providing help and clarifications with various cosmological concepts throughout.

#### References

- [1] Perlmutter, S. et al. (1999) ‘Measurements of  $\Omega$  and  $\Lambda$  from 42 high-redshift supernovae’, *The Astrophysical Journal*, 517(2), pp. 565–586. doi:10.1086/307221.
- [2] Riess, A.G. et al. (1998) ‘Observational evidence from supernovae for an accelerating universe and a cosmological constant’, *The Astronomical Journal*, 116(3), pp. 1009–1038. doi:10.1086/300499.
- [3] Velten, H.E., vom Marttens, R.F. and Zimdahl, W. (2014) ‘Aspects of the cosmological “coincidence problem”’, *The European Physical Journal C*, 74(11). doi:10.1140/epjc/s10052-014-3160-4.
- [4] Suzuki, N. et al. (2012) ‘The Hubble Space Telescope Cluster Supernova Survey. V. Improving the Dark-Energy Constraints above  $z > 1$  and Building an Early-type-hosted Supernova Sample’, *The Astrophysical Journal*, 746(1), p. 85. doi:10.1088/0004-637x/746/1/85.
- [5] Betoule, M. et al. (2014) ‘Improved cosmological constraints from a joint analysis of the SDSS-II and SNe Supernova samples’, *Astronomy & Astrophysics*, 568. doi:10.1051/0004-6361/201423413.
- [6] Scolnic, D. et al. (2022) ‘The pantheon+ analysis: The Full Data Set and light-curve release’, *The Astrophysical Journal*, 938(2), p. 113. doi:10.3847/1538-4357/ac8b7a.
- [7] Abbott, T.M. et al. (2019) ‘First cosmology results using type 1a supernovae from the Dark Energy Survey: Constraints on cosmological parameters’, *The Astrophysical Journal Letters*, 872(2). doi:10.3847/2041-8213/ab04fa.
- [8] Planck Collaboration (2020) ‘Planck 2018 results’, *Astronomy & Astrophysics*, 641. doi:10.1051/0004-6361/201833910.
- [9] Beutler, F. et al. (2011) ‘The 6dF Galaxy Survey: Baryon acoustic oscillations and the local Hubble constant’, *Monthly Notices of the Royal Astronomical Society*, 416(4), pp. 3017–3032. doi:10.1111/j.1365-2966.2011.19250.x.
- [10] Baade, W. (1938) ‘The absolute photographic magnitude of supernovae.’, *The Astrophysical Journal*, 88, p. 285. doi:10.1086/143983.
- [11] Codata value: Newtonian constant of gravitation. Available at: <https://physics.nist.gov/cgi-bin/cuu/Value?bg> (Accessed: 11 March 2024).
- [12] CODATA value: Speed of light in vacuum. Available at: <https://physics.nist.gov/cgi-bin/cuu/Value?c> (Accessed: 11 March 2024).
- [13] Camarena, D. and Marra, V. (2016) ‘Cosmological constraints on the radiation released during Structure formation’, *The European Physical Journal C*, 76(11). doi:10.1140/epjc/s10052-016-4517-7.
- [14] Bandyopadhyay, T. and Debnath, U. (2019) ‘Parameterizing dark energy models and study of finite time future singularities’, *Advances in High Energy Physics*, 2019, pp. 1–12. doi:10.1155/2019/5393491.
- [15] Shtanov, Y. and Sahni, V. (2010) ‘Generalizing the cosmic energy equation’, *Physical Review D*, 82(10). doi:10.1103/physrevd.82.101503.
- [16] Ottoson, T.A. (2012) ‘Markov-Chain Monte-Carlo: A Bayesian Approach to Statistical Mechanics’, doi://doi.org/10.48550/arXiv.1206.6905
- [17] Yang, W. et al. (2020) ‘Dynamical Dark Energy after planck CMB final release and  $H_0$  tension’, *Monthly Notices of the Royal Astronomical Society*, 501(4), pp. 5845–5858. doi:10.1093/mnras/staa3914.

**Scientific Summary for a General Audience**

Cosmology is the study of the origin and evolution of our Universe, and as such, it is of great interest and importance. Theories about the structure of the Universe have been proposed for centuries, spearheaded by Albert Einstein's Theory of General Relativity in 1917, in which Einstein introduced the idea of a 'cosmological constant' to maintain a static universe - the general consensus at the time. This idea was later quashed by Edwin Hubble's measurements of the redshift of nearby galaxies in 1929, which strongly suggested an expanding Universe, leading to Einstein infamously describing the cosmological constant as his "biggest blunder". However, it was later found that the expansion of the Universe is accelerating, and the cosmological constant was reintroduced in a different form - to represent the 'vacuum energy' or 'dark energy' - to account for this. As the name suggests, the 'cosmological constant' is a model in which the density of dark energy in the Universe does not change with time. But what if the density of dark energy is not a constant?

This paper investigates several dynamical dark energy models, in which the dark energy density varies with time, to determine any viable, alternative models to the cosmological constant.

## Appendix A: Further Plots

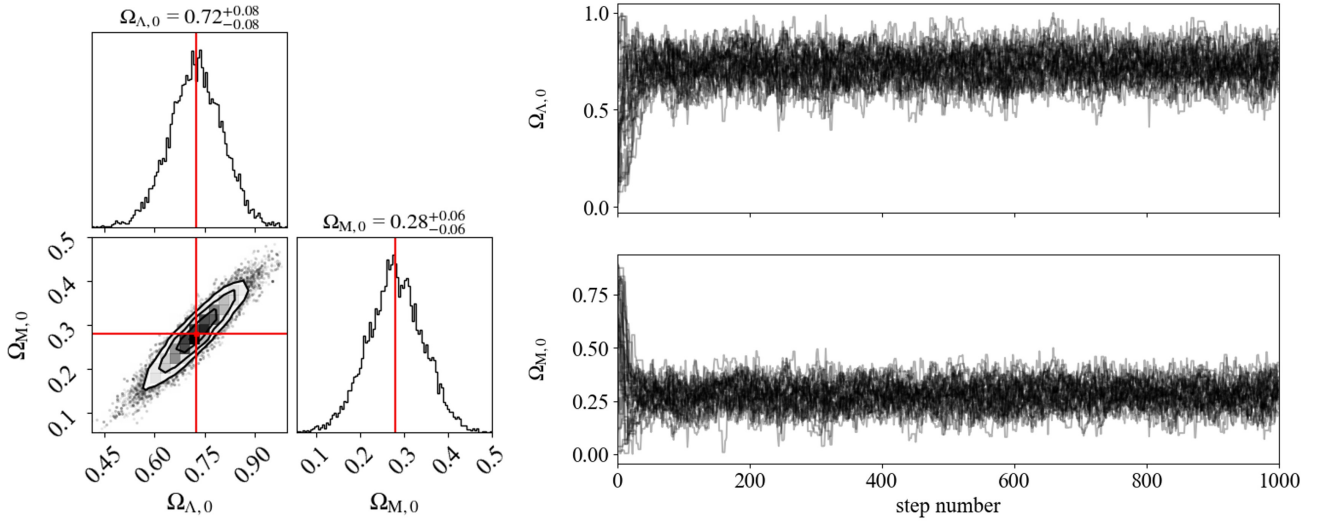


**FIG. 5.** Constraints on the  $\Lambda$ CDM dark energy model with uniform priors and no restriction on Universe geometry. Left: The MCMC corner plot showing contour plots to illustrate the correlation between parameters, with contours at 0.5, 1, 1.5, and 2 standard deviations, as well as marginalised posterior probability distributions for each parameter. The red lines indicate the 50th percentile. Right: The position of each random walker as a function of the number of steps, illustrating the convergence of the MCMC algorithm after around 100 steps.

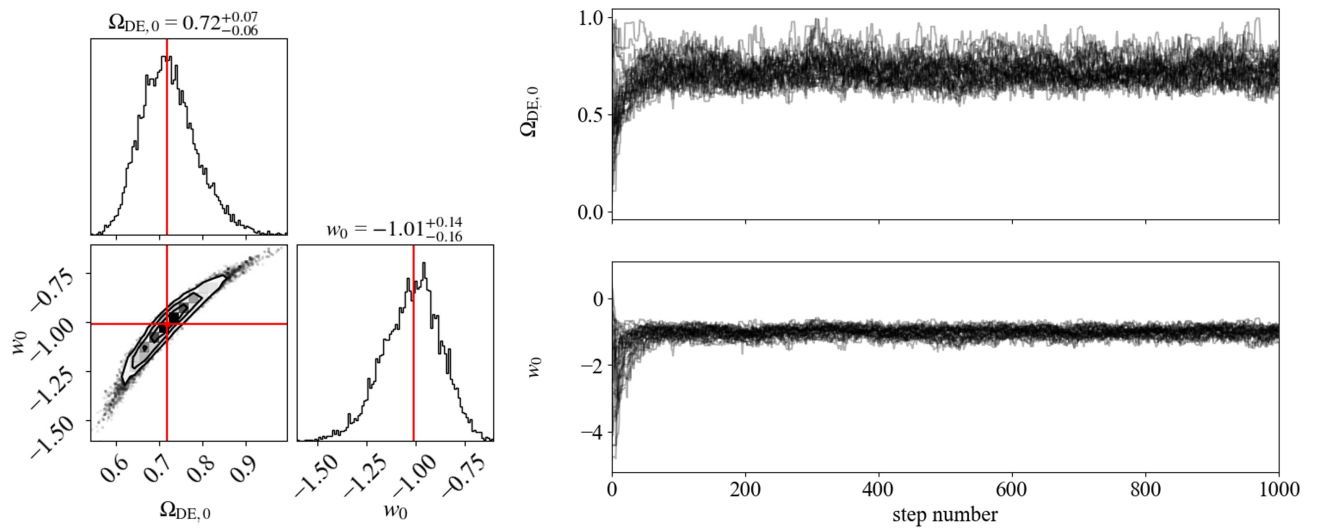


**FIG. 6.** Constraints on the  $w$ CDM dark energy model with uniform priors under the assumption of a flat Universe. Left: The MCMC corner plot showing contour plots to illustrate the correlation between parameters, with contours at 0.5, 1, 1.5, and 2 standard deviations, as well as marginalised posterior probability distributions for each parameter. The red lines indicate the 50th percentile. Right: The position of each random walker as a function of the number of steps, illustrating the convergence of the MCMC algorithm after around 100 steps.

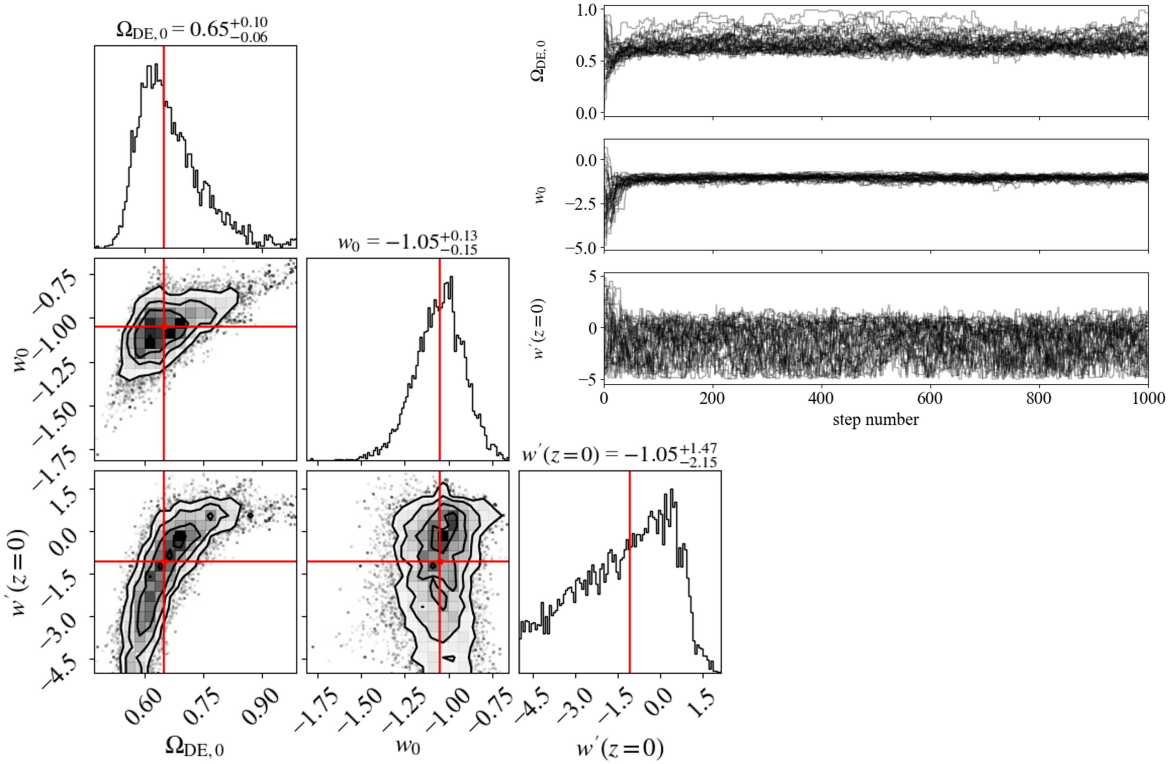


**FIG. 7.** Constraints on the CPL dark energy model with uniform priors under the assumption of a flat Universe. Left: The MCMC corner plot showing contour plots to illustrate the correlation between parameters, with contours at 0.5, 1, 1.5, and 2 standard deviations, as well as marginalised posterior probability distributions for each parameter. The red lines indicate the 50th percentile. Right: The position of each random walker as a function of the number of steps, illustrating the convergence of the MCMC algorithm after around 100 steps.

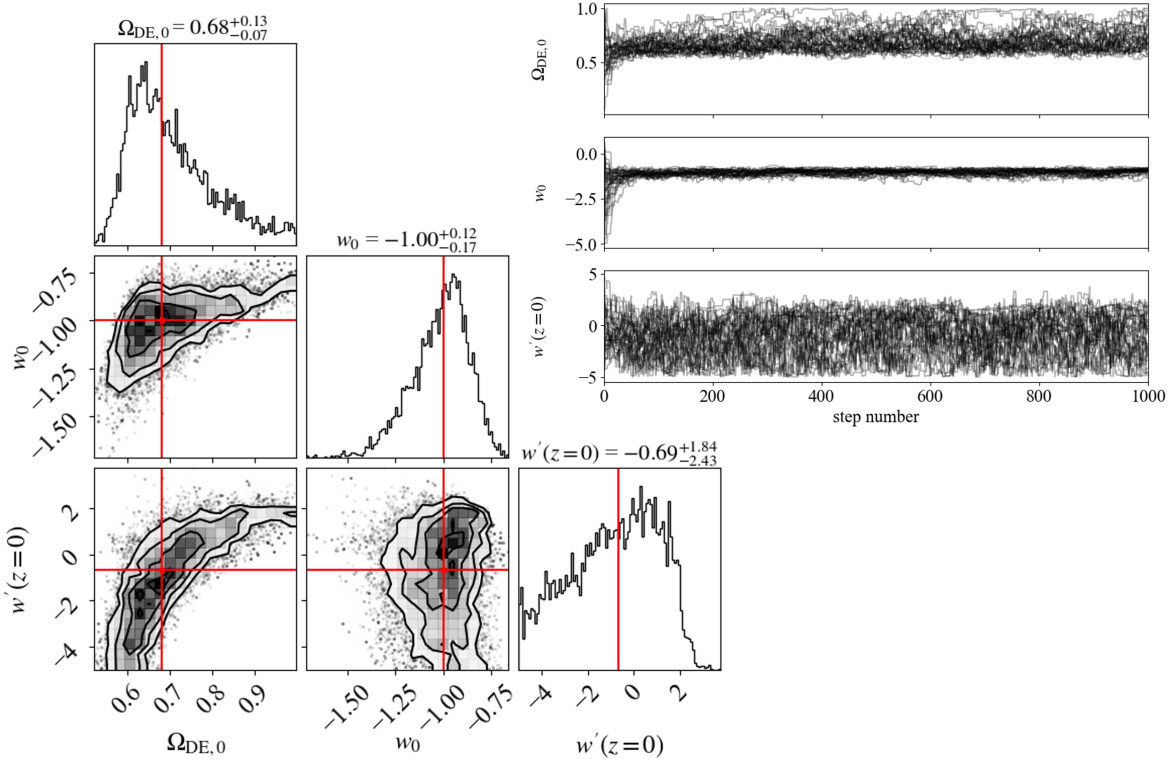


**FIG. 8.** Constraints on the JBP dark energy model with uniform priors under the assumption of a flat Universe. Left: The MCMC corner plot showing contour plots to illustrate the correlation between parameters, with contours at 0.5, 1, 1.5, and 2 standard deviations, as well as marginalised posterior probability distributions for each parameter. The red lines indicate the 50th percentile. Right: The position of each random walker as a function of the number of steps, illustrating the convergence of the MCMC algorithm after around 100 steps.

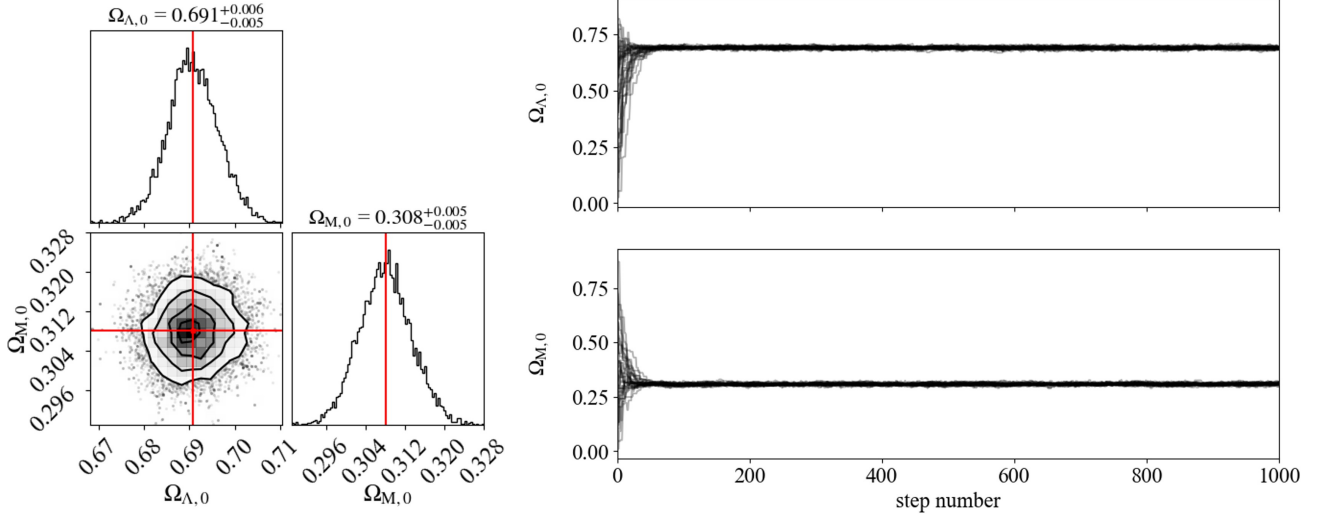


**FIG. 9.** Constraints on the  $\Lambda$ CDM dark energy model with CMB+BAO priors and no restriction on Universe geometry. Left: The MCMC corner plot showing contour plots to illustrate the correlation between parameters, with contours at 0.5, 1, 1.5, and 2 standard deviations, as well as marginalised posterior probability distributions for each parameter. The red lines indicate the 50th percentile. Right: The position of each random walker as a function of the number of steps, illustrating the convergence of the MCMC algorithm after around 100 steps.

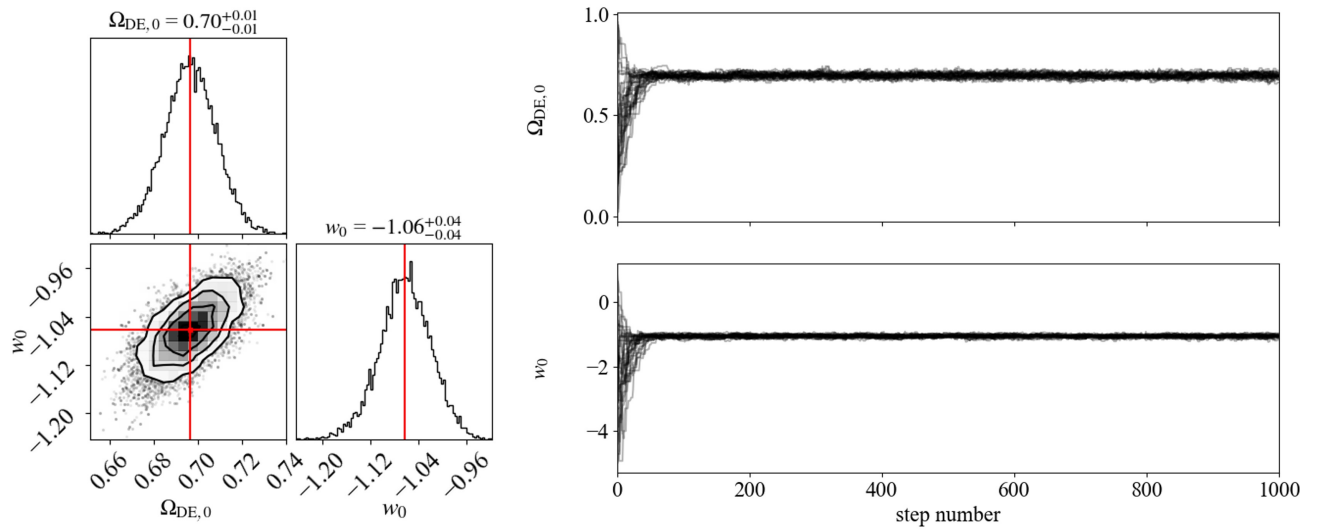


**FIG. 10.** Constraints on the  $w$ CDM dark energy model with CMB+BAO priors under the assumption of a flat Universe. Left: The MCMC corner plot showing contour plots to illustrate the correlation between parameters, with contours at 0.5, 1, 1.5, and 2 standard deviations, as well as marginalised posterior probability distributions for each parameter. The red lines indicate the 50th percentile. Right: The position of each random walker as a function of the number of steps, illustrating the convergence of the MCMC algorithm after around 100 steps.

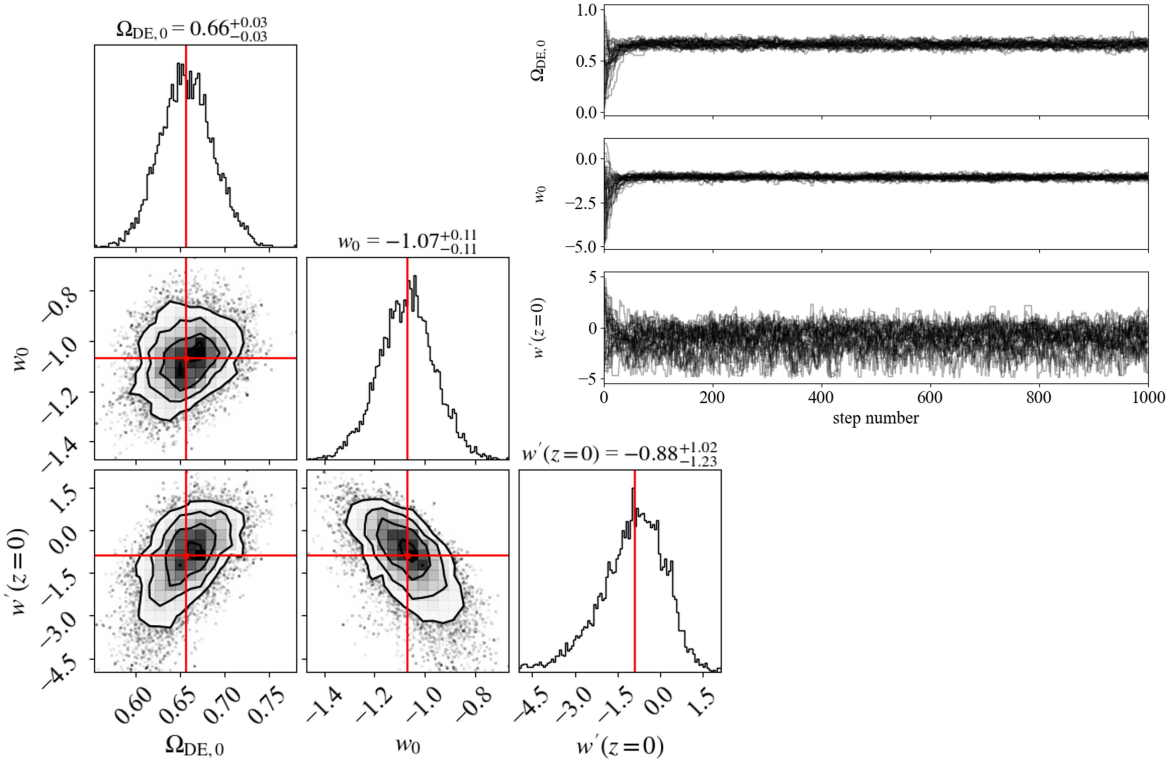


**FIG. 11.** Constraints on the CPL dark energy model with CMB+BAO priors under the assumption of a flat Universe. Left: The MCMC corner plot showing contour plots to illustrate the correlation between parameters, with contours at 0.5, 1, 1.5, and 2 standard deviations, as well as marginalised posterior probability distributions for each parameter. The red lines indicate the 50th percentile. Right: The position of each random walker as a function of the number of steps, illustrating the convergence of the MCMC algorithm after around 100 steps.

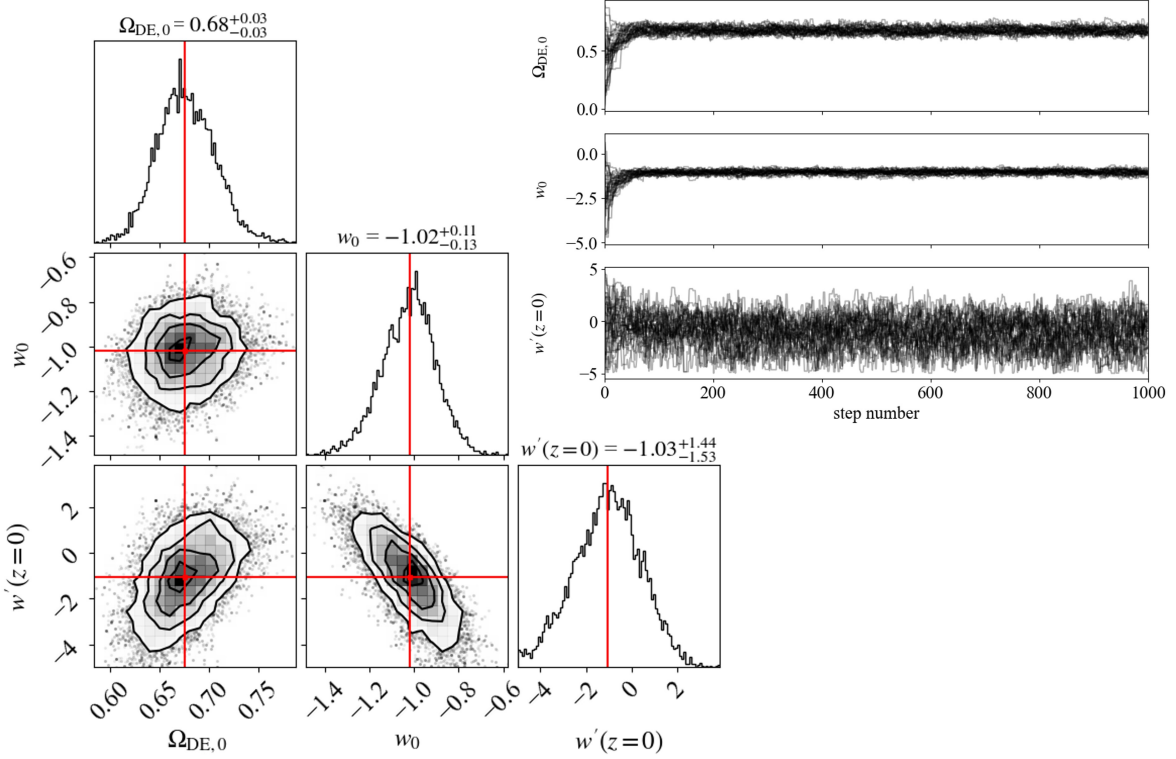


**FIG. 12.** Constraints on the JBP dark energy model with CMB+BAO priors under the assumption of a flat Universe. Left: The MCMC corner plot showing contour plots to illustrate the correlation between parameters, with contours at 0.5, 1, 1.5, and 2 standard deviations, as well as marginalised posterior probability distributions for each parameter. The red lines indicate the 50th percentile. Right: The position of each random walker as a function of the number of steps, illustrating the convergence of the MCMC algorithm after around 100 steps.

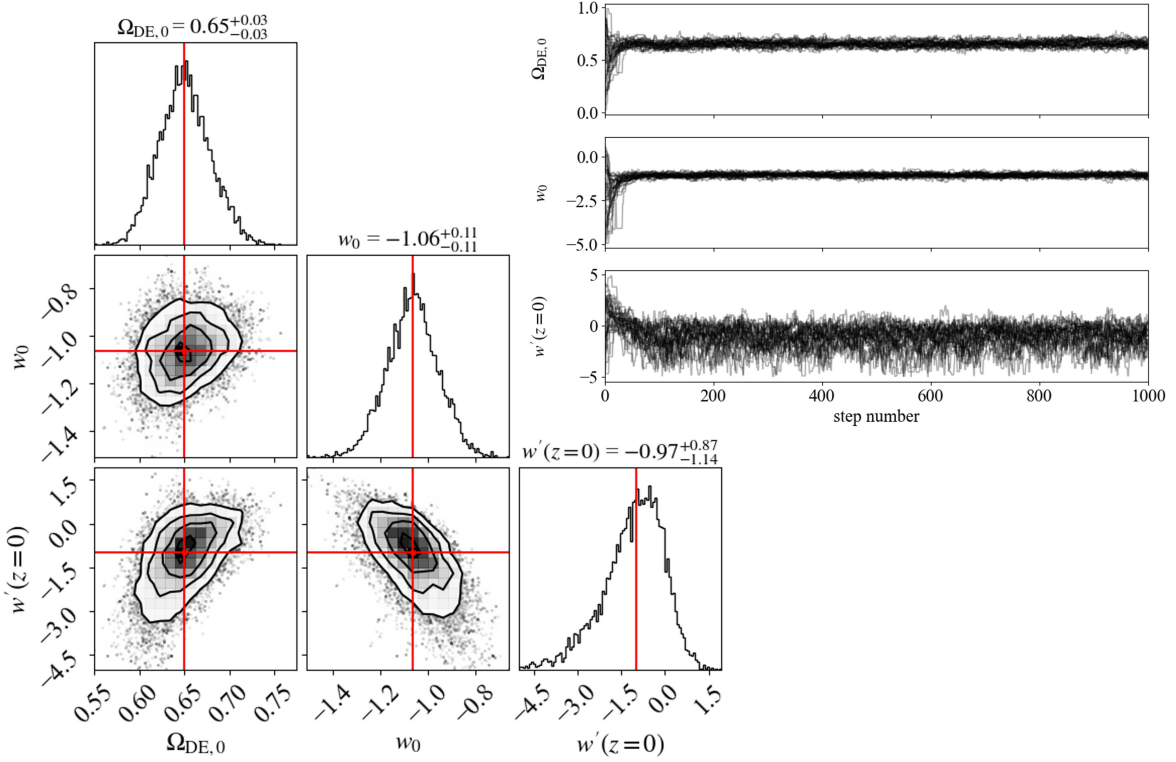


**FIG. 13.** Constraints on the Efstathiou dark energy model with CMB+BAO priors under the assumption of a flat Universe. Left: The MCMC corner plot showing contour plots to illustrate the correlation between parameters, with contours at 0.5, 1, 1.5, and 2 standard deviations, as well as marginalised posterior probability distributions for each parameter. The red lines indicate the 50th percentile. Right: The position of each random walker as a function of the number of steps, illustrating the convergence of the MCMC algorithm after around 100 steps.